

Size dependence of lateral quantum-confinement effects of the optical response in $\text{In}_{0.53}\text{Ga}_{0.47}\text{As}/\text{InP}$ quantum wires

M. Notomi,* S. Nojima, M. Okamoto, H. Iwamura, and T. Tamamura

NTT Opto-electronics Laboratories, 3-1 Morinosato-Wakamiya, Atsugi, Kanagawa 243-01, Japan

J. Hammersberg and H. Weman

Department of Physics and Measurement Technology, Linköping University, S-581 83 Linköping, Sweden

(Received 3 January 1995)

The size dependence of various aspects of quantum-confinement effects in $\text{In}_{0.53}\text{Ga}_{0.47}\text{As}/\text{InP}$ quantum wires was quantitatively examined through photoluminescence experiments with and without magnetic field, along with theoretical calculation. The wires were fabricated by combining electron-beam lithography and reverse-mesa wet etching, thus enabling us to easily control the lateral size independently of the vertical size. Photoluminescence experiments showed distinct peak shifts with changes in the lateral size and showed a shoulder structure that is attributed to laterally quantized second subbands. The energy shift of both levels is explained by a detailed theoretical calculation that incorporates conduction-band nonparabolicity, valence-band coupling, and excitonic correction. The lateral quantum confinement is also demonstrated by the magnetic-field effect on the luminescence spectrum, in which we can distinguish the lateral quantum effects from other factors. As magnetic-field strength increases, a transition from quantum-confined subbands to Landau subbands was clearly observed for first and second subbands. At high excitation levels, the quenching of higher Landau levels was observed. In-plane and perpendicular-to-plane anisotropy of polarization in luminescence was also investigated and the size dependence of this anisotropy in both directions is largely explained by the calculated lateral confinement effect of the optical-transition matrix elements. The phenomenon observed for narrower wires, however, cannot be explained by our theory and is thought to be due to wave-function localization.

I. INTRODUCTION

Two-dimensional quantum-confined structures, called quantum-well wires (QWW's), are innovative materials potentially applicable in optical devices such as laser diodes.^{1,2} Although lateral patterning in the required sizes (typically 10–15 nm) has been difficult by using electron-beam (EB) lithography or thin-film growth techniques, progress in lithographic technology and the combination of several other techniques are making it possible to fabricate QWW's that exhibit some quantum-confinement effects in various ways: etching and regrowth,^{3–5} selective growth,^{6,7} growth on tilted substrates,^{8,9} and growth on V -grooved substrates.¹⁰

Various quantum-confinement effects, such as the photoluminescence (PL) wavelength blueshift and the appearance of quantized levels, have been extensively studied in quantum-well films (QWF's). These studies considered the quantum-confinement size (i.e., well width) to be an important parameter in investigating quantum effects. On the other hand, although several studies have addressed quantum-confinement effects, such as the PL-wavelength blueshift and polarization anisotropy in QWW's, there have been few studies of investigations into the quantum-confinement effect in QWW's while varying the lateral size.

This is because in QWW's it is difficult to control the lateral size systematically within the range from the

weak-confinement regime (around 100 nm) to the strong-confinement regime (less than 20 nm). Moreover, changes in lateral size are often accompanied by changes in vertical size, making any observed change a mixture of the effects of changes in the lateral and vertical sizes, and making it difficult to investigate the quantum-confinement effect quantitatively. For most methods not using lithographic techniques, the final size is small enough, but it is difficult to vary the lateral size independently of the vertical size. EB lithography, on the other hand, provides better control of wire size, but the final size is larger than required. Furthermore, wires fabricated by a combination of EB lithography and dry etching are likely to be damaged during the fabrication process.

We therefore used a combination of EB lithography and reverse-mesa selective wet etching to fabricate QWW's for the purpose of quantitatively investigating the effects of lateral quantum confinement on their optical properties. EB lithography allowed us to control the lateral size easily, and using sequential selective etching for the $\text{In}_{0.53}\text{Ga}_{0.47}\text{As}/\text{InP}$ material system enabled us to overcome the side-etching problem inherent in wet etching. Reverse-mesa wet etching is a key process because it forms wires smaller than can be formed by EB lithography without fatal damage,^{11–13} and simultaneously smooths variations in wire width.¹⁴ Even with minor damage from wet etching and overgrowth, the fabricated wires retain sufficient optical quality for luminescence ex-

periments. By this method, we successfully fabricated optically active QWW's small enough for the quantum confinement by systematically controlling the lateral size.

In this paper, we investigate the transition energy of QWW's in a PL experiment. We quantitatively clarify changes in the transition energy and the appearance of laterally quantized levels, which are well-known quantum-confinement effects in QWF's but which have not yet been investigated in detail in QWW's. We also carefully calculate the lateral confinement effect and compare the calculated results with experimental results.

We then investigate the lateral confinement effects in a magneto-PL experiment. The magnetic field can be used as a probe for the quantum-confinement effects because it causes magnetic confinement which competes with the quantum confinement.^{15–18} Application of a magnetic field is especially effective for multidimensional quantum-confined structures, since it lets us investigate effects from only *lateral* confinement in the Faraday configuration. We examine the magnetic-field effect on PL spectra to determine how the magnetic field affects the lateral confinement effects.

We also investigate the polarization characteristics. The polarization property of QWW's, in contrast to that of QWF's, has been predicted to depend on the wire's cross-sectional shape.¹⁹ In other words, polarization properties are expected to vary when the cross-sectional shape is changed. Although several papers have reported in-plane anisotropy for quantum wires,²⁰ to our knowledge the polarization of quantum wires has not been studied while varying the cross-sectional size. We inspect this dependence for various wire sizes and in two orientations (perpendicular-to-plane and in-plane). To clarify the quantum-confinement effect, we compare the experimental results with theoretical calculations. Part of this study has already been published in brief letters.^{12,13,21}

II. SAMPLES

This section briefly summarizes the sample fabrication procedure; a detailed description can be found elsewhere.^{12,13} The fabrication flow is illustrated in Fig. 1. A line-and-space resist pattern (typical pitch 150 nm) was written in the [110] direction by high-resolution electron-beam lithography on a lattice matched $\text{In}_{0.53}\text{Ga}_{0.47}\text{As}/\text{InP}$ single-quantum-well wafer grown by gas-source molecular-beam epitaxy then several sequences of selective wet etching were used to form an $\text{In}_{0.53}\text{Ga}_{0.47}\text{As}$ quantum wire structure at the bottom of the reverse mesa of InP [shown in Fig. 1(e)]. Due to the selective anisotropic (reverse-mesa-shaped) etching techniques used, we obtained a very uniform 10-nm-scale quantum wire structure, a size beyond the limit of present lithography. The wires were then buried within InP by metal-organic vapor-phase epitaxy in order to improve their optical characteristics [Fig. 1(f)]. Typical high-resolution scanning-electron-microscope (SEM) photographs are shown in Fig. 2 for wires before (a) and after [(b) and (c)] overgrowth are shown in Figs. 2.

For the PL experiments, several sets of wire patterns exposed at different EB doses were prepared on each sam-

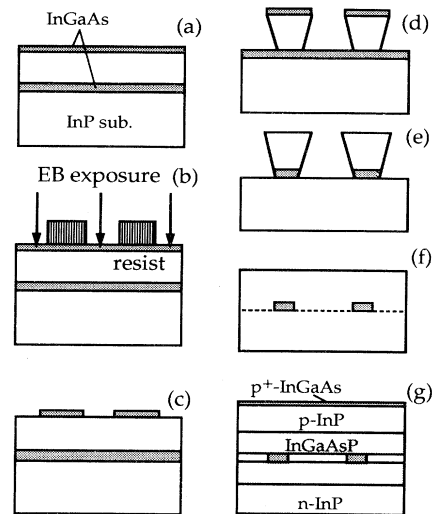


FIG. 1. Schematic of the fabrication process for $\text{In}_{0.53}\text{Ga}_{0.47}\text{As}/\text{InP}$ quantum wires.

ple. The typical pattern was $300 \times 300 \mu\text{m}^2$. An unetched region outside the wire pattern was etched off by additive lithography in order to discriminate the signal from that of the unprocessed QWF region. Each pattern was mesa shaped a few micrometers deep, and a sufficient number of reference patterns were left unetched near the wire patterns.

For the electroluminescence experiments, the wires were located within a *pn* junction and sandwiched between $\text{In}_{0.83}\text{Ga}_{0.17}\text{As}_{0.36}\text{P}_{0.64}$ waveguide layers as shown in Fig. 1(g). Figure 2(d) shows a typical SEM photograph of these samples. We used a conventional device fabrication process to form mesa-stripe structures having electrodes. The typical stripe length was $700 \mu\text{m}$, and the wire was parallel to the stripe for all samples.

III. SIZE DEPENDENCE OF TRANSITION ENERGY

A. Experimental setup and luminescence efficiency

The excitation light source we used was an argon-ion laser operating at 514.5 nm, and focused onto a spot approximately $300 \mu\text{m}$ in diameter. The excitation power ranged from $10 \mu\text{W}$ to 5 mW, and was typically $300 \mu\text{W}$. The samples were placed in a liquid-helium cryostat, and PL signals were detected by conventional lock-in technique using a cooled Ge photodetector.

To evaluate the overall quality of QWW's produced by our method, we studied the PL intensity from the QWW's. We detected sufficient intensity even from the narrowest wires, only 10 nm wide. The fact that 10-nm-wide wires can still emit intense luminescence shows that our fabrication process does not cause fatal damage in the etched and regrown heterointerfaces.

The integrated PL intensity relative to wire widths is shown in Fig. 3 with the intensity normalized by the area of the wires. The normalized intensity is nearly constant

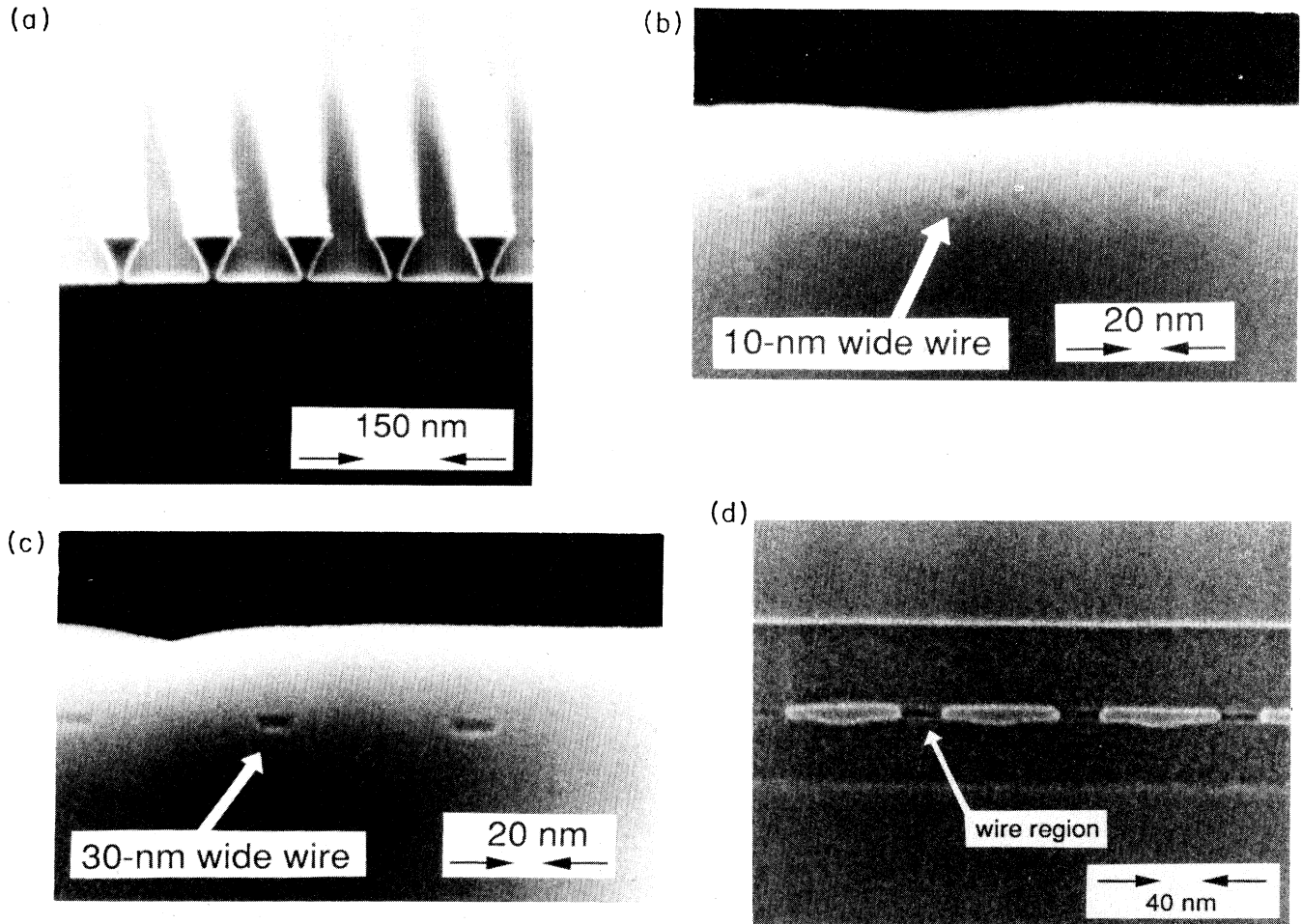


FIG. 2. SEM cross-sectional views of $\text{In}_{0.53}\text{Ga}_{0.47}\text{As}/\text{InP}$ quantum wires. As-etched 10-nm-wide quantum wires (a). Buried 10-nm-wide (b) and 30-nm-wide (c) quantum wires. Quantum wires within the waveguide layer (d).

for wires between 35 and 60 nm wide, and decreases for those less than 30 nm wide. This decrease in luminescence intensity might be due to the nonradiative recombination centers. In the case of 30-nm-wide wires, the overgrowth process increased PL intensity threefold to fivefold. The results in Fig. 3 contrast greatly with those for dry-etched wires,²² whose PL intensity decreases rapidly at widths less than 100 nm. This suggests that the process damage is quite low with our etching-and-regrowth procedure. We also think that this low process damage can be attributed in part to the characteristics of InP-based materials.²³ They should have a lower surface recombination velocity and be more suitable for regrowth than other materials, such as $\text{GaAs}/\text{Al}_x\text{Ga}_{1-x}\text{As}$.

The integrated PL intensity is shown in Fig. 4 as a function of excitation power for various wire widths. Over four orders-of-magnitude variation in excitation power, the PL intensity is directly proportional to the excitation power. This indicates that there is no involvement of extrinsic factors (such as impurity levels) and suggests an intrinsic-nature recombination.

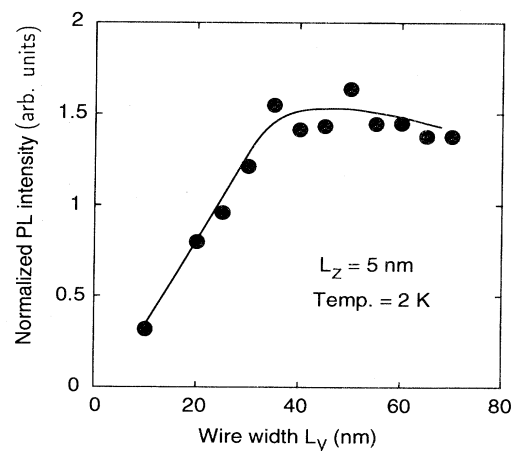


FIG. 3. Normalized PL intensity vs wire width for 5-nm-thick wires. The normalized intensity is nearly constant for wire widths down to 35 nm.

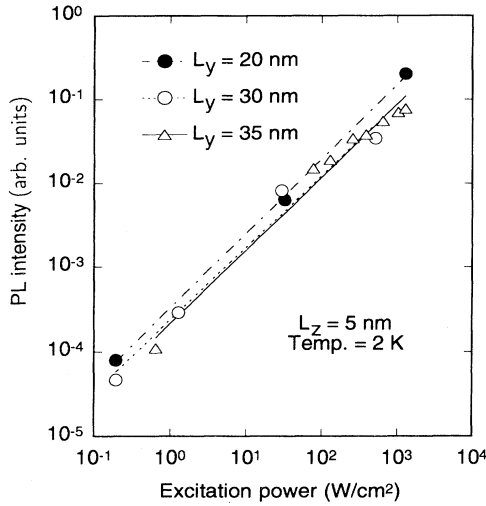


FIG. 4. Excitation-power dependence of normalized PL intensity for 5-nm-thick wires of various widths. In all cases, all the data points are either on or near the same linear curve representing the excitation levels over four orders of magnitude.

B. Photoluminescence energy shift

We next investigated relationships between the wire width and the shape and peak wavelength of the PL spectrum. Figure 5 shows the typical PL spectra at 2 K for 5-nm-thick $\text{In}_{0.53}\text{Ga}_{0.47}\text{As}/\text{InP}$ QWW's of three lateral widths. The PL peak energy of the 50-nm-wide wires is close to that of the reference QWF's, and the PL peak clearly shifts to shorter wavelengths (i.e., a blueshift) for narrower wires. This shift reaches a value of 40 meV for 10-nm-wide wires. A similar blueshift of the PL peak was observed in all the QWE's fabricated in our laboratory,

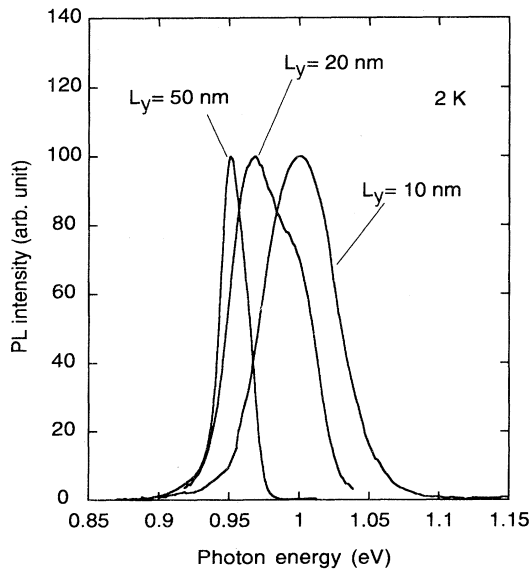


FIG. 5. PL spectra of 5-nm-thick quantum wires of various widths.

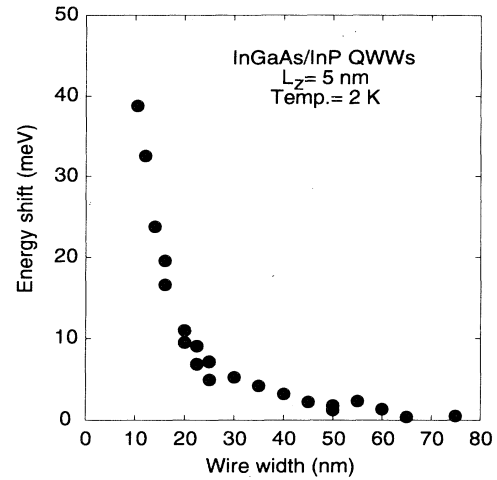


FIG. 6. Energy shift of the PL peak from that of a QWF (solid circles) vs wire width for 5-nm-thick wires. The error bars in the size determination is approximately the diameter of the circles.

irrespective of the thickness of the $\text{In}_{0.53}\text{Ga}_{0.47}\text{As}$ well and the InP cap.

Several factors in addition to quantum-confinement effects may be responsible for this shift of the PL peak: band-gap distribution in the original QWF, strain caused by overgrowth of the mesa structure, and impurities introduced in the fabrication process. To find out whether this blueshift is evidence of the quantum confinement, it is therefore important to determine the magnitude of the shift precisely, and to compare it with the calculated lateral quantum-confinement effect.

We measured the distribution of the PL wavelength in the as-grown QWF wafer in order to avoid the influence of the in-plane distribution in the original QWF. Wire widths for the same samples that were used for the PL measurements were directly evaluated by a high-resolution SEM. We determined the wire-width value for each pattern by averaging the measured values from a sufficient number of wires so as to avoid any effects of size fluctuation.

The energy-shift data thus obtained are plotted in Fig. 6 against widths. The energy shift increases as wire size decreases, as expected from the quantum-confinement effect. To evaluate this quantitatively, we next calculate the wire-size dependence of the transition energy of quantum wires.

C. Calculation of transition energy

1. Numerical method

It is not difficult to estimate the transition energy of QWF's by a simple calculation, especially for thicknesses over 10 nm. We have only to solve a one-dimensional (1D) Schrödinger equation assuming a parabolic-band approximation. Although this simplification is frequently also used for quantum wires, this treatment can result in

significant errors. Our aim in this section is to investigate the wire-size dependence of the transition energy accurately, and to compare the calculated dependence with the experimental data. In what follows, we assume x , y , and z axes along the $[110]$, $[\bar{1}10]$, and $[001]$ orientations. The x' , y' , and z' axes used for a Hamiltonian matrix are oriented in $[100]$, $[010]$, and $[001]$.

A frequently used approximation is obtained by decoupling the y and z quantization,²⁴ leading to two sets of 1D Schrödinger equations with a 1D potential $V(z)$. Because the above approximation is valid only for wide wires, where the aspect ratio of the cross section is large enough, we instead directly solve 2D Schrödinger equations using the 2D potential $V(y,z)$. A calculation procedure is done by expanding the wave function using a series of plane waves.²⁵

In our previous paper and in other papers, a parabolic-band approximation is used to account for the energy level of quantum wires. Although this approximation can give a proper estimation for a QWF energy level for conduction and valence bands when the film thickness is more than 10 nm, it has not proved true for quantum wires even if sizes are larger than 10 nm. Therefore, we next consider nonparabolic effects for the conduction and valence bands.

2. Nonparabolicity in the conduction band

In the present work, the vertical (L_z) confinement is always strong, which leads to a quantization energy of approximately 100 meV. This confinement energy causes a large enhancement of the effective mass for the conduction band, the so-called nonparabolicity effect.^{26–18} For QWF's, this effect is only significant in explaining the energy level of very thin films. For quantum wires, however, this mass enhancement caused by z confinement can affect the y confinement even if the wire width is large. Conduction-mass enhancement for quantum wires was recently indicated by tight-binding calculation²⁹ and by the nonparabolicity consideration.³⁰ Here we assume the nonparabolicity effect is a function only of the z -confinement energy, because z confinement is always larger than y confinement in our samples. We used a nonparabolic term for the $\text{In}_{0.53}\text{Ga}_{0.47}\text{As}/\text{InP}$ system developed by Wetzal *et al.* in Ref. 27.

We assume a square potential for the conduction band, and that the mass discontinuity is adequately taken into account. The material parameters used³¹ are listed in Table I. We used 15×15 plane waves to expand wave functions, which were confirmed enough for convergence. Figure 7(a) shows the energy shift of the conduction band

TABLE I. Material parameters used in the energy-level calculation for $\text{In}_{0.53}\text{Ga}_{0.47}\text{As}/\text{InP}$ quantum wires. s.o. denotes spin-orbit splitting.

	m_c^*	m_{hh}^*	γ_1	γ_2	γ_3	s.o. (meV)
$\text{In}_{0.53}\text{Ga}_{0.47}\text{As}$	0.0416	0.3807	13.6	5.42	6.29	361
InP	0.0077	0.65	4.95	1.65	2.35	130

with changing L_y for parabolic and nonparabolic cases. The nonparabolicity effect for the conduction band causes a slight decrease in blueshift due to the quantization energy of the z confinement. Note that since we ignored nonparabolicity from the y confinement, this decrease is underestimated especially for narrow wires, but that the discrepancy must be small because z -confinement energy is always larger than y -confinement energy for all wire sizes of our samples.

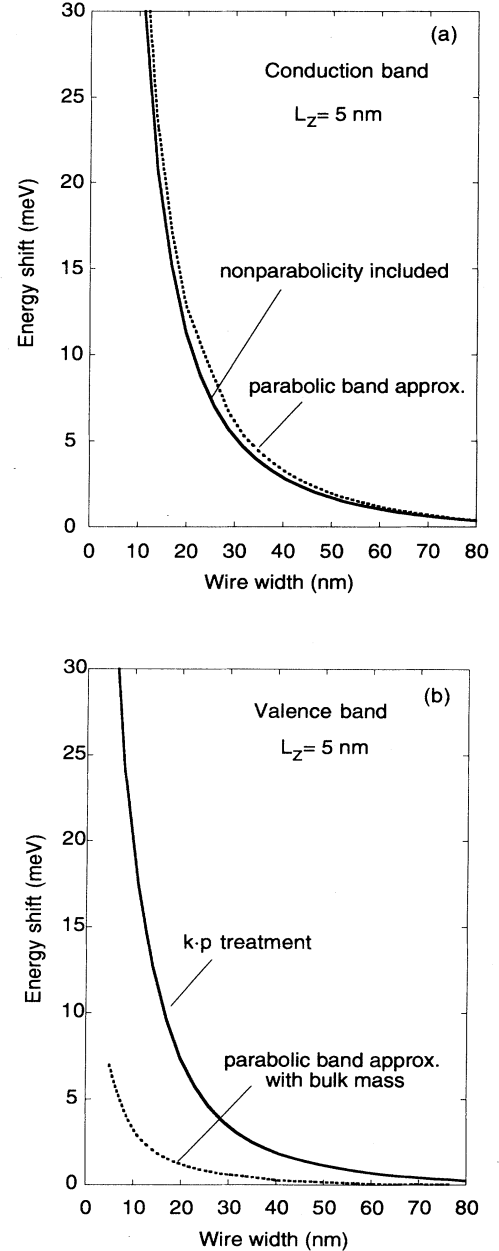


FIG. 7. Calculated energy level of conduction band (a), and valence band (b) for 5-nm-thick quantum wires. Solid lines are obtained with nonparabolicity (a) and the $\mathbf{k} \cdot \mathbf{p}$ method (b). Broken lines are obtained with the isotropic parabolic band model.

3. *k*·*p* treatment of valence subbands

For (001) QWF's, valence bands at the zone center can be precisely described by two decoupled parabolas: heavy hole and light hole. If we want to evaluate an energy level of the topmost valence band, we can use a parabolic-band model with a heavy-hole mass. If the anisotropy of the valence bands is taken into account, we can construct the heavy-hole and light-hole masses for any index of substrates for Luttinger parameters. Especially for (001) QWF's, the heavy-hole mass for the (001) direction, which gives a confinement mass, is close to the bulk heavy-hole mass. Therefore, the parabolic-band treatment with a bulk mass is a good approximation for QWF's. For quantum wires, however, the situation is very different. Consider $L_z < L_y$. The *z* confinement induces a large splitting between two valence bands and makes the $J_z = \frac{3}{2}$ band (*heavy-hole-like* band) topmost, where J_z is an angular momentum projected along the *z* axis. This results in the so-called *mass reversal effect* for the in-plane mass. Thus the effective mass for the *y* direction of the $J_z = \frac{3}{2}$ band is close to bulk *light-hole* mass. This means that light-hole mass is more adequate in accounting for the energy shift of holes induced by the lateral confinement. However, a simple anisotropic

effective-mass model—bulk heavy-hole mass for the strong confinement direction and bulk light-hole mass for the weak confinement direction—is also incorrect because the effect of valence-band coupling is significant for quasi-1D systems even at the zone center. The quasi-1D valence subbands are mixture states of $J_z = \frac{1}{2}$ and $J_z = \frac{3}{2}$, where mixing is dominated by the quantum confinement. When $L_z \ll L_y$ —that is, when the mixing is not strong—the quantization energy shift by L_y is dominated by the in-plane heavy-hole mass of (001) QWF's. As L_y decreases, the splitting between the heavy-hole-like state ($J_z \approx \frac{3}{2}$) and the light-hole-like state ($J_z \approx \frac{1}{2}$) decreases, because the energy shift of the former is larger than that of the latter. As a result, coupling between these two states is enhanced. Therefore, we have to solve a multi-band Hamiltonian matrix in which the mixing effect is correctly taken into account. Recently, tight-binding analysis also showed that the valence-band mass is reduced for quantum wires.³²

We solved a 6×6 Hamiltonian matrix constructed from a 3×3 *k*·*p* Hamiltonian and a 6×6 spin orbit interaction Hamiltonian in which the coupling of the three valence bands is taken into account.³³ A Hamiltonian matrix of (110)-oriented quantum wires is given by (neglecting a spin-orbit part)

$$H_{kp}^v = \frac{\hbar^2}{m_0} \begin{pmatrix} Lk_x^3 + M(k_y^2 + k_z^2) & Nk_x k_y & Nk_z k_x \\ Nk_x k_y & Lk_y^2 + M(k_z^2 + k_x^2) & Nk_y k_z \\ Nk_z k_x & Nk_y k_z & Lk_z^2 + M(k_x^2 + k_y^2) \end{pmatrix} \begin{pmatrix} |X'\rangle \\ |Y'\rangle \\ |Z'\rangle \end{pmatrix}, \quad (1)$$

where

$$\begin{pmatrix} k_x' \\ k_y' \\ k_z' \end{pmatrix} = \begin{pmatrix} 0 & 0 & -1 \\ -1/\sqrt{2} & 1/\sqrt{2} & 0 \\ 1/\sqrt{2} & 1/\sqrt{2} & 0 \end{pmatrix} \begin{pmatrix} -i\partial/\partial x \\ -i\partial/\partial y \\ k_z \end{pmatrix}, \quad (2)$$

and $L = \gamma_1 + 4\gamma_2$, $M = \gamma_1 - 2\gamma_2$, and $N = 6\gamma_3$.

This Hamiltonian was expanded by 15×15 plane waves as was done for the conduction-band calculation, and diagonalized to obtain eigenvalues. The calculation procedure was, except for the Hamiltonian matrix, the same as that used for the conduction band.

Figure 7(b) shows the energy shift of the topmost valence band with the parabolic approximation using the bulk heavy-hole mass, and with the multiband Hamiltonian matrix. These curves differ significantly. The energy shift of the valence band is greatly enhanced, especially for wide wires, due to a mass reduction in the *y* direction. It is apparent that the parabolic-band model is not adequate for *all* wire sizes. Therefore, the treatment in Ref. 12 is not adequate, especially for wide wires.

4. Excitonic correction

In the above calculation, we neglected the excitonic effect; that is, the effect of the electron-hole Coulomb interaction. This effect should be size dependent and more

pronounced for narrow wires, as it is for QWF's. We calculated the binding energy of the exciton in QWW's by using the variational method. We ignored the valence-band coupling effect and used the same parameters we used in the energy-level calculation.

Although a trial function for excitons is usually assumed to be a hydrogen-atom-like wave function, such a function has singularity at the origin in the one-dimensional case. Thus we have to use modified trial functions. We solved the problem by a variational method using the trial function

$$\phi(z) = \phi_0 \exp[-\sqrt{(z/\lambda)^2 + \sigma^2}], \quad (3)$$

where λ and σ are variational parameters. This function is a smooth function at the origin, and asymptotically approaches the Whittaker function (the ideally one-dimensional case) for large *z*. The form of Eq. (3) has been shown³⁴ to be more accurate over a wide range of QWW sizes than previously reported functions.^{35,36} Concerning the Coulomb potential, we used an effective 1D Coulomb potential³⁷ which was obtained by integration in *x* and *y* coordinates using eigenfunctions of quantum wire.

Figure 8 shows the calculated binding energy of a one-dimensional exciton in 5-nm-thick $\text{In}_{0.53}\text{Ga}_{0.47}\text{As}/\text{InP}$ QWW's as a function of wire width. The binding energy for all wire sizes is found to be enhanced over that of

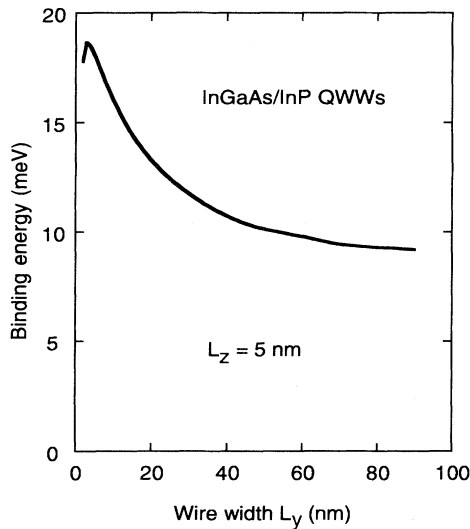


FIG. 8. Calculated exciton binding energy of 5-nm-thick $\text{In}_{0.53}\text{Ga}_{0.47}\text{As}/\text{InP}$ quantum wires vs the wire width.

QWF's, and a maximum enhancement of 10 meV is obtained at a width of about 5 nm. The decrease in binding energy in narrower wires is attributed to the overflow of wave functions from the well.

D. Comparison with experimental results

The sum of the subband energy levels of the conduction and valence bands, and of an excitonic correction, gives the transition energy of QWW's. The calculated transition energy with and without the excitonic effect is shown by the broken and solid lines in Fig. 9 versus the wire width. It is clear that the overall profile of the experimental data is close to both of the calculated curves—we will consider the difference between the two theoretical curves later. This indicates that the observed shift is induced mainly by the lateral quantum-confinement effect—not by such factors as strain and impurity levels. If these factors did make a major contribution to the observed shift, the curves would not coincide with the data because the wire-size dependence of these factors would be different from that in the above calculation.

When focusing on the difference between the two curves, the broken line appears to be closer to the experimental results than the solid line. This implies that the observed shift originates from a combination of the lateral confinement and the excitonic effect. In this experiment, the largest contribution to the error bar comes from the wire-size determination (a few nanometers). This uncertainty might produce an error bar on an energy scale larger than 10 meV when $L_z \approx 10$ nm. The error bar in the energy scale for wider wires, however, should be small (less than 1 meV). The discrepancy for wide wires without excitonic correction therefore cannot be explained by size uncertainty. Better fitting with the excitonic effect for the present analysis means that we observe a wire-size-dependent excitonic effect in the PL en-

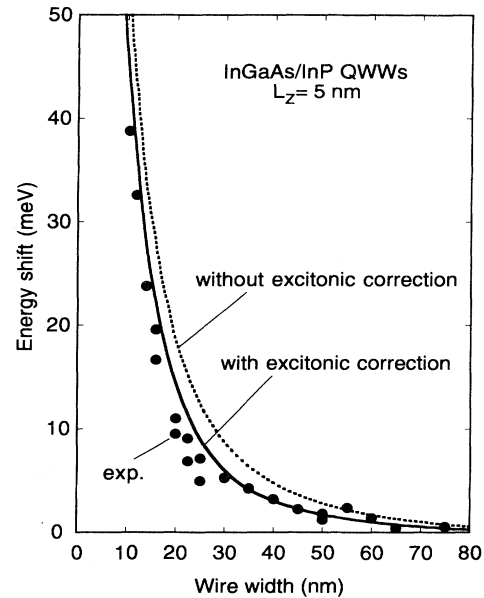


FIG. 9. Energy levels for 5-nm-thick $\text{In}_{0.53}\text{Ga}_{0.47}\text{As}/\text{InP}$ quantum wires calculated with (solid line) and without (broken line) excitonic effects. Circles are the same experimental results plotted in Fig. 6.

ergy shift. In our previous report (Ref. 12), we obtained a good fitting without excitonic correction. This is because we used a parabolic-band approximation which causes the error in estimation mentioned in Sec. III C. The present analysis shows that the excitonic correction is necessary to explain the transition-energy shift in QWW's.

Consequently, we think that the overall nature of the measured blueshift is, with the excitonic effect calculated here, quantitatively explained by the lateral quantum confinement, including the band nonparabolicity.

E. Higher subband structures

We observed distinctive shoulder structures in PL spectra like those shown in Fig. 5 on the high-energy side of the peak for 15–50-nm-wide wires. We regard these as due to laterally quantized subbands. In QWF's, one clear demonstration of the quantum-confinement effect was the appearance of laterally quantized subband levels.^{38,39} Here we investigate these structures by theoretical calculation. Figure 10 shows the wire-width dependence of the shoulder structures. To distinguish variations in the shoulder from the PL peak shift, the peaks for QWW's with different widths are superimposed. This figure demonstrates that the shoulder separates from the main peak as the wire becomes narrower. A shoulder structure commonly appears for wires 15–50 nm wide.

The measured energy levels of the shoulders are plotted in Fig. 11 as solid circles against the wire widths. The energy of a shoulder structure, determined from deconvolution, clearly shifts higher, in a manner similar to the PL peak. This wire-size dependence of the shoul-

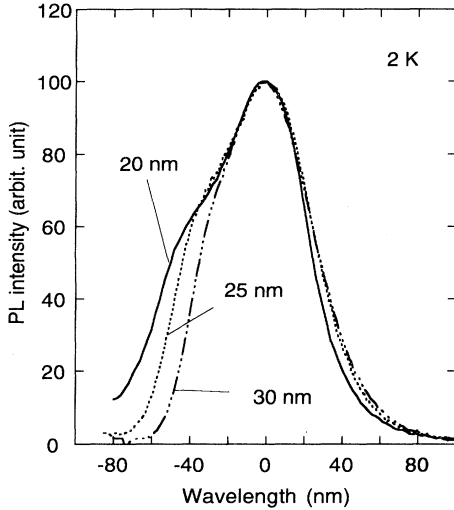


FIG. 10. Shoulder structures observed in the PL spectra of 5-nm-thick quantum wires of various widths. The peaks of the PL spectra are superimposed in order to clarify the variance in the shoulder structures. The shoulder shifts to a shorter wavelength as the wire width decreases.

der structures reminds us of the transition associated with the higher subbands of QWW's.

To investigate this, we calculated the subband energy levels of QWW's using the method described in Sec. III C. The results show that the energy position of the shoulders is very close to the first subband level of the QWW's, denoted $12H$. $12H$ represents the transition associated with the topmost hole subband where the quantized number on the z axis is 1 and that on the y axis is 2. The calculated energy level for $12H$ is shown in Fig. 11

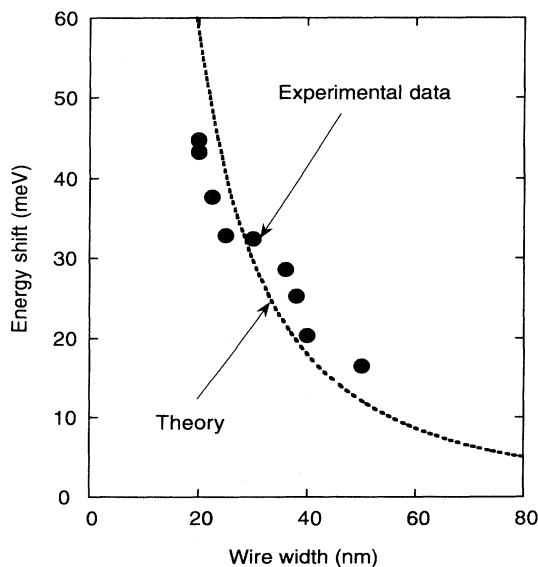


FIG. 11. PL energy shift of the shoulder structures (solid circles) vs wire width. The dashed line represents the first excited level ($12H$) calculated theoretically.

by the dashed curve, and fairly good agreement between the experimental and calculated data is observed: the variation according to wire size is well explained by the calculation. This suggests that the shoulder is related to the first lateral-quantized subband, and that the energy shift of the shoulder is caused by the change in the lateral confinement. This agreement is additional evidence that the lateral confinement is achieved in the fabricated QWW's. No shoulder structures appeared in the PL spectrum of the 10-nm wires. We assume this is because, in the 10-nm wires, the energy level of the first subband is too high to be populated by carriers, or because the lifetime of the excited carriers was too short to accumulate carriers at the excited levels. This assignment of these shoulder structures will be further supported by a magneto-optical study developed in Sec. IV.

IV. MAGNETO-OPTICAL STUDY

In Sec. III, we investigated the wire-size-dependent energy shift in photoluminescence spectra, and found that comparison between measured and calculated values indicates that the whole shift is caused by the lateral confinement effect in QWW's. In this section, we examine the origin of this shift by using a magnetic field as a probe of the quantum-confinement effect, and obtain further evidence of lateral quantization in the wires.

In this experiment, a continuous magnetic field was applied in the Faraday configuration, where the magnetic field is parallel to the growth axis (z axis). The temperature was kept at 1.8 K. The samples were excited by an Ar-ion laser with the light coupled to an optical fiber, and the same fiber was used for detecting the luminescence. Other experimental details were the same as outlined in previous sections of this paper.

Figure 12 shows the PL spectra of four 5-nm-thick wires ($L_y = 20, 25, 35,$ and 45 nm) at 14 and 0 T. The shift in peak energy with changing wire width is apparently less pronounced than when no magnetic field is applied. To see this more clearly, we plotted the energy shift with and without a magnetic field against the wire width in Fig. 13. This figure shows that the blueshift is suppressed by the magnetic field.

The magnetic field induces a two-dimensional confinement of harmonic-oscillator potential perpendicular to the magnetic field. If the potential confinement exists, both types of confinement will couple. In the present configuration, the magnetic-field quantization couples only with the lateral potential quantization, and the magnetic field can therefore be used as a probe of the lateral confinement. This situation is analogous to cases involving a QWF with a magnetic field parallel to the well.⁴⁰

If the lateral potential can be approximated as a harmonic-oscillator potential ($\hbar\omega_0$), the energy level is obtained analytically⁴¹ as

$$E_n = (n + \frac{1}{2})\sqrt{(\hbar\omega_B)^2 + (\hbar\omega_0)^2}, \quad (4)$$

where $\omega_B = eB/m^*$. According to this relation, if $\omega_B \gg \omega_0$, then E_n becomes almost independent of ω_0 . The cyclotron diameter of the ground Landau level at 14 T is approximately 13 nm, which is less than the present wire

width. This means that the magnetic quantization should, at this magnetic-field strength, dominate the quantum-wire quantization. Thus, if the blueshift of the ground-level peak is caused by the lateral confinement, the present magnetic field should make it disappear.

The suppression of the blueshift observed in Fig. 13 can hence be explained as the transition from the lateral quantum-confined regime to the magnetically confined regime. Here the lateral potential confinement is most strongly coupled with the magnetic field. If the blueshift has other origins—vertical confinement effect, strain, or other extrinsic factors—it would be unchanged after applying a magnetic field. Consequently, we can exclude such factors for the observed energy shift.

Equation (4) is not a good approximation in this case, however, because the lateral potential is not a harmonic type. To evaluate the magnetic effect quantitatively, we assumed a realistic square potential and numerically calculated the energy levels of QWW's with presence of the magnetic field. The magnetic field was incorporated as a vector potential using a conventional Landau gauge, and the eigenvalues were obtained through the plane-wave expansion method in the same way as in the energy-level calculation. The calculated curve is shown in Fig. 13. The suppression of the blueshift is well explained by this calculation, indicating that it results from competition between the lateral confinement and the magnetic confinement. This confirms that the observed shift is caused by the lateral quantum-confinement effect.

So far we discussed only the single-particle quantization affected by a magnetic field, but it is well known that a diamagnetic shift is markedly influenced by a change of Coulomb interaction between electrons and holes in the presence of a magnetic field. In our results, this diamagnetic shift of excitons (i.e., Coulombic correction) should be involved in the difference between cases with and without magnetic field. The discussion in Sec. III, however, concluded that the wire-width dependence of the transition energy is determined mainly by the wire-width dependence of the single-particle quantization energy—at least at widths greater than 20 nm. In other words, the wire-width dependence of the exciton binding energy does not play a major role if we see the change of transition energy. Since the wire-width dependence of the Coulombic correction must be scaled with that of the exciton binding energy, the wire-width dependence observed in Fig. 13 can be basically explained, as a first approximation, in terms of the single-particle quantization.⁴² Although low-dimensional excitons under a magnetic field are also a theoretically interesting problem, we ignore this aspect here. A detailed discussion of the magnetic-field-induced energy shift is left for a future work.

Another clear demonstration of the lateral confinement effect was given through a magneto-PL experiment. Figure 14 shows PL spectra at 14 T at high excitation levels (10 W/cm^2 : more than two orders of magnitude higher than in the previous experiment). A dense carrier filling can easily be achieved without using extremely intense pulsed excitation because the carrier diffusion is suppressed by the deep mesa structure and also by the la-

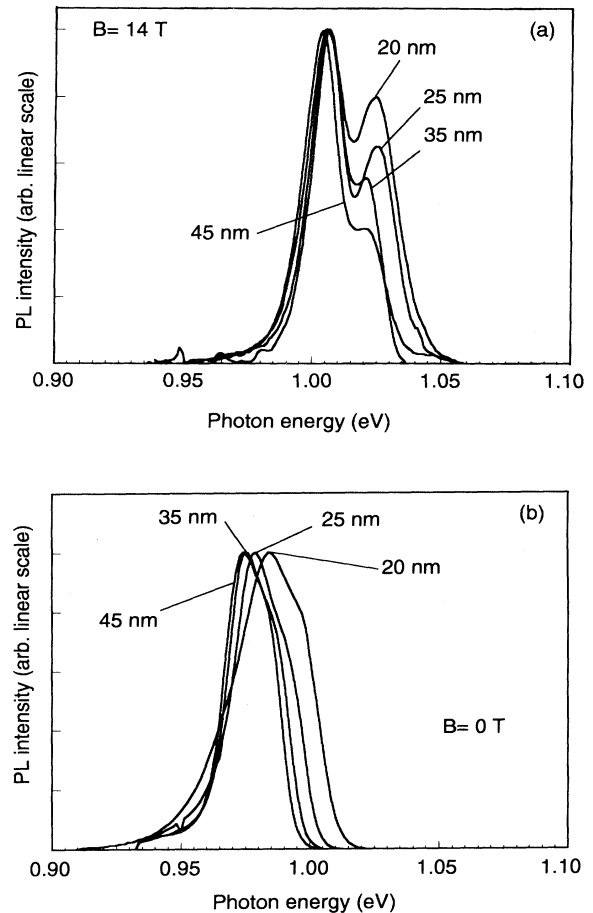


FIG. 12. Magneto-PL spectra of four different widths of 5-nm-thick quantum wires in the Faraday configuration at (a) 14 T and (b) 0 T.

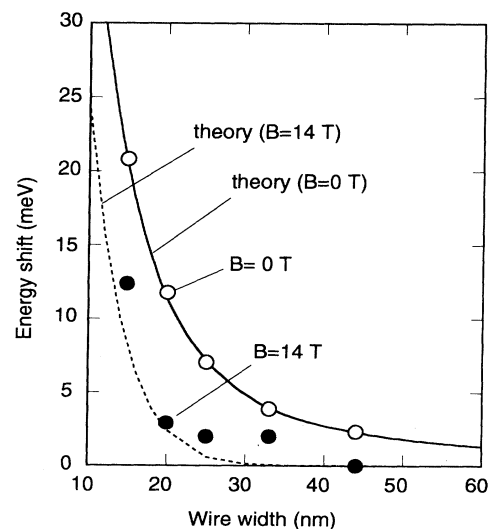


FIG. 13. Energy shift of the ground-state levels vs the wire width at 14 and 0 T. The calculated energy shifts incorporating the magnetic field are shown as the broken curve (14 T) and the solid curve (0 T).

teral potential itself. The figure shows that approximately 100 meV of the quasi-Fermi level is realized for all wires. Five Landau levels can be seen in the 45-nm-wide wires, and the highest Landau level is close to the Fermi edge, which is quite reasonable. Although the quasi-Fermi level determined from the width of the PL spectra is almost the same for all the wires, the number of Landau levels decreases as the wire width decreases. For 20-nm-wide wires, there are only two Landau levels. This is not due to changes in level occupation, because it is obvious that carriers populate beyond the second Landau level. This means higher Landau levels might be affected by the lateral confinement.

We regard this phenomenon as a quenching of Landau levels. The diameter of the n th Landau orbit of a free electron within a magnetic field is given by $2R_c = 2\sqrt{\hbar(2n+1)/eB}$. If the n th Landau orbit is larger than the wire width, the electron cannot form the closed orbit, and the Landau level is thus unobservable. Although the basic mechanism is similar to the magnetic depopulation in a 1D system observed by Shubnikov-de Haas oscillation measurement,⁴³ to our knowledge there have been no previous reports on the quenching of the Landau level in photoluminescence experiments.

Strictly speaking, true Landau levels exist only at the high-field limit. As the field strength decreases, the Landau levels continuously join with the laterally quantized subbands. This is straightforwardly understood if we

consider a harmonic potential like that given in Eq. (4). Therefore, if the magnetic energy becomes less than the confinement energy, we expect to observe the laterally quantized subbands instead of Landau levels. In our case, however, the higher subbands ($13H$, $14H$, and so on) are difficult to observe because they suffer from lateral size inhomogeneity, whereas the Landau levels are not affected by it. This is why we see quenching of Landau levels. If we had perfect wires, we would see a crossover from the field-dependent Landau levels to the field-independent subbands. The calculated cyclotron diameters for free electrons are 13, 22, and 29 nm for the three lowest Landau levels. While it seems impossible to form the second Landau level in the 20-nm-wide wires, the crossover is not as abrupt as expected from Eq. (4).

For the case of $n=1$ Landau levels, however, we clearly observe the crossover from Landau levels ($n=1$) to laterally quantized subbands ($12H$), instead of a quenching of Landau levels. As discussed in Sec. III, we observe laterally quantized subbands for 15–50-nm wide wires. If we decrease the magnetic-field strength, second Landau levels are continuously joined with shoulder structures present at 0 T.

These results demonstrate that application of magnetic field causes a transition from a quantum-confined region to a magnetically confined region. Next, we investigate the magnetic-field dependence of subbands and Landau levels to see this crossover more clearly. Figure 15 shows

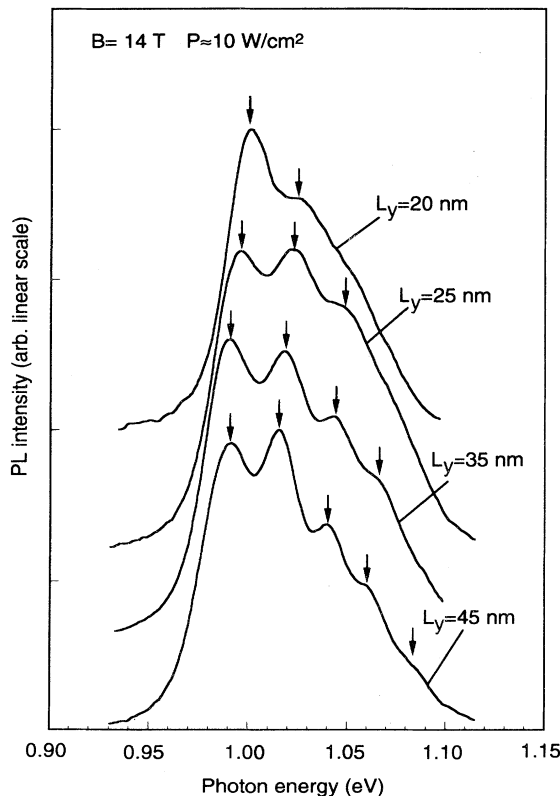


FIG. 14. High-excitation magneto-PL spectra of four different widths of 5-nm-thick quantum wires at 14 T. Arrows point at assigned Landau levels.

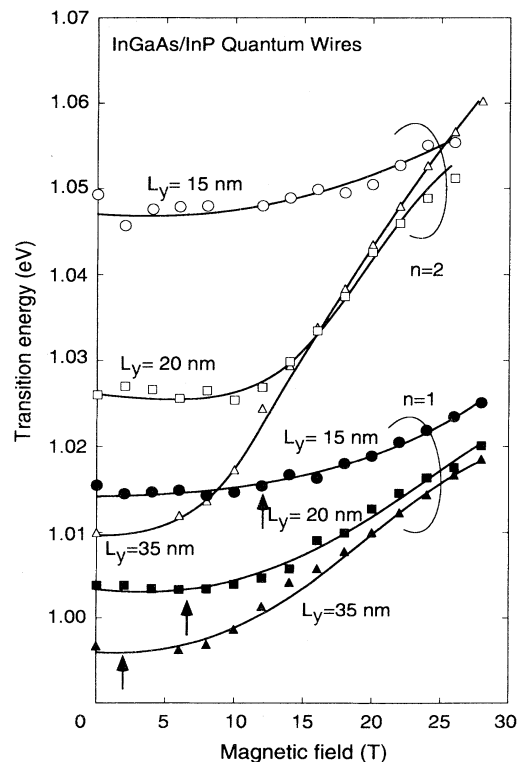


FIG. 15. Transition energy of a ground state ($n=0$, filled symbols) and a first excited state ($n=1$, open symbols) vs magnetic fields for 5-nm-thick quantum wires of three different widths. Arrows mark the magnetic fields at which the cyclotron diameter coincides with the lateral dimension of wires.

the energy position of resolved peaks for three different wires versus magnetic field. Lowest ($n=0$) and second lower ($n=1$) peaks are plotted. Peaks were deconvoluted through the Gaussian fitting.

First, look at curves of the lowest transition for each wire (filled symbols). Although curves for wide wires are nearly linear similar to QWF's, as expected for typical Landau fans, curves for narrower wires become flattened at low field. Apparently, a crossover from a linear curve to a flattened curve occurs at a higher field for narrower wires. Excitonic correction is also known to cause deviation from linear dependence at low fields for QWFs,^{44,45} but the crossover due to the excitonic effect should occur at a smaller field corresponding to exciton binding energy (typically 10 meV). In this case, crossover occurs at very high field, which cannot be explained by the excitonic correction discussed in Sec. III C 4. Arrows point at the magnetic field at which the cyclotron diameter coincides with the lateral confinement size. The arrows are fairly close to the crossover points, indicating that this crossover occurs as a result of the lateral confinement effect. Therefore, this flattened region is the quantum-confinement-dominated region, as mentioned above.

Next, look at the second subbands, which show a similar trend of crossover from linear to flattened. At zero field, this second peak is assigned to the second laterally quantized subband ($12H$) from the energy-level calculation in Sec. III, and at high field the peak shape becomes that of a typical Landau subband ($n=1$) in magneto-PL spectra. This means that the crossover occurs between laterally quantized subbands and Landau levels in this case. As mentioned above, laterally quantized subbands should be continuously connected to Landau subbands as the field increases. This is an unambiguous demonstration that shoulders observed at zero-field PL spectra are due to lateral quantum confinement. Note that the crossover energy is higher for higher subbands. At near critical field, electrons of the first subband have a quasi-one-dimensional character, whereas electrons of the second subband have a quasi-two-dimensional one. Concerning higher subbands ($n>2$), we can only observe Landau subbands at sufficiently high fields. At fields lower than a critical value, we observe the disappearance of Landau levels, as discussed above. Consequently, the crossover (or disappearance) of each subband is determined by the lateral size of wires and the size of the Landau orbit.

To calculate theoretically the magnetic-field dependence of higher subbands with the square-well potential, we have to incorporate an accurate treatment of the magnetic-field dependence of the valence bands and the nonparabolicity effect in the conduction band. Note that a harmonic-type approximation like Eq. (4) is not adequate to analyze the subband structures quantitatively under a magnetic field. The detailed analysis will be done in a future study.

In this section, we confirmed through magneto-PL experiment that the energy shift observed in Sec. III is caused by *lateral* quantum confinement. Furthermore, we found that shoulders in PL spectra which were assigned as laterally quantized subbands ($12H$) in Sec. III are continuously connected to second Landau subbands ($n=1$)

at higher fields, and that higher Landau levels ($n>1$) are quenched in narrow QWW's. All these crossovers are determined by the relation between the lateral dimension of wires and the size of the Landau orbit.

V. SIZE DEPENDENCE OF POLARIZATION

A. Experimental setup

As mentioned above, the polarization of QWW's should strongly depend on the cross-sectional shape. We should therefore be able to control the polarization anisotropy by changing the ratio of the lateral width to the vertical width. Here we investigate the polarization anisotropy in luminescence while varying the lateral wire width. When characterizing polarization, we have to be careful of a few things. If the vertical dimension of wires is much smaller than the lateral dimension, the QWW polarization might be very close to that of QWF's. This is important because the smallest lateral width is much larger than the vertical width in our fabrication method. In addition, when we examine the polarization property, it is advantageous to use the well region within the waveguide layer. A thin well layer without a waveguide layer might exhibit a complicated mixture of signals with different orientations. We therefore used relatively thick (15 nm) wire samples each having a waveguide layer.

We performed two kinds of luminescence anisotropy experiments. The first was an edge-emitted electroluminescence (EL) experiment, in which we examined the perpendicular-to-plane anisotropy. (We also measured the edge-emitted PL for several samples, but this was more difficult than for the surface-emitted configuration because the patterned area is so small.) The other was a surface-emitted PL experiment, in which we examined the in-plane anisotropy. We used samples with the same structure for both experiments.

Figure 16 shows the experimental configurations adopted for the polarization-resolved measurement. As shown in Fig. 16(a), we collected EL signals from the cleaved facet, where the measured EL is always parallel to the wires. From these, we evaluated the perpendicular-to-plane polarization of EL. Figure 16(b) shows the configuration for the surface-emitted PL experiment in which we analyzed the polarization of the luminescence by rotating a polarizer in front of the monochromator. The polarization dependence of the measurement equipment was carefully canceled out using a depolarizer.

B. Anisotropy in edge-emitted EL

We measured the polarization-resolved EL spectra for quantum films and quantum wires at 7 K. The luminescence from the QWF is strongly polarized in TE, similar to the reported polarization anisotropy of QWF's,⁴⁶ but we found that TE polarization decreased for narrower wires. The TM/TE ratio of the EL peak intensity (solid circles) is plotted in Fig. 17 as a function of the wire width (L_y). The injection current was kept at 10 μ A. The TM/TE ratio increases as L_y decreases, and ap-

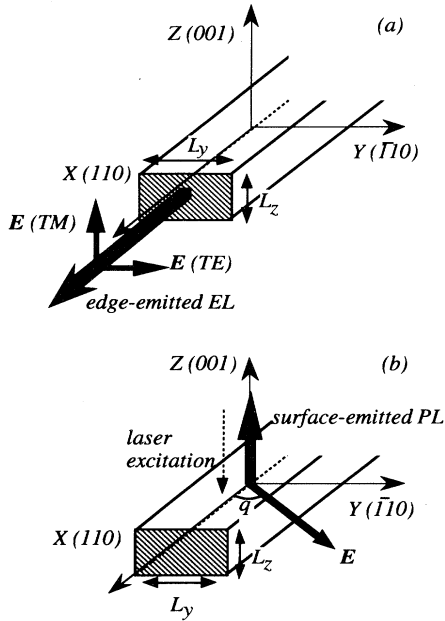


FIG. 16. Schematics of the polarization-resolved experimental configurations for (a) the edge-emitted EL and (b) the surface-emitted PL experiments.

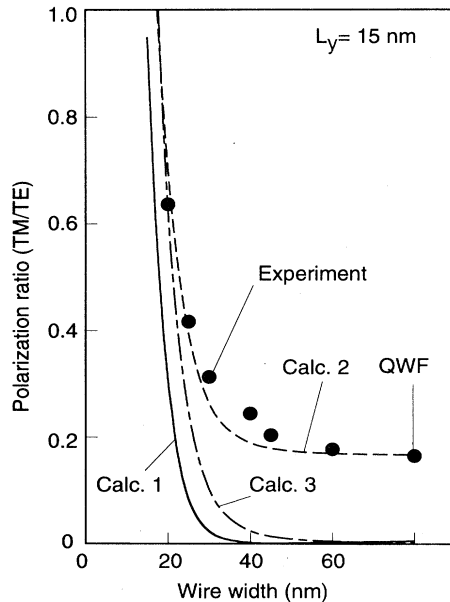


FIG. 17. Measured polarization ratio (TM/TE) in edge-emitted EL for 15-nm-thick quantum wires as a function of wire widths with an injection current of $10 \mu\text{A}$ at 7 K. The ratio is determined from the peak intensity of EL spectra. Curves calculated are also plotted (calcs. 1–3) using three models described in the text.

proaches a value of 1.0. This tendency is consistent with that expected for the quantum-confinement-induced polarization change, since QWW's having a symmetrical cross section ($L_y = L_z = 15 \text{ nm}$) should emit unpolarized luminescence in an edge-emitting geometry if we ignore the intrinsic anisotropy of the crystal structure.

We also investigated the injection-current dependence of EL polarization. Figure 18 shows three spectra taken at different current injection levels. The spectra and polarization characteristics are similar at currents of $20 \mu\text{A}$ and 1 mA, but the spectrum shape changes dramatically and the polarization property becomes complicated at currents over 2 mA. This indicates that the luminescence signal reflects only the ground-state transition for currents less than 1 mA. The complicated nature of high-current-injection levels might result from their complicated valence-subband structures. Therefore, the polarization anisotropy in Fig. 17 reflects the property of the ground state of the valence band which possesses a heavy-hole-like character. This is because the current level ($10 \mu\text{A}$) and the sample temperature (7 K) are low enough. In fact, the spectral shape itself is almost identical between those of TE and TM at this low current, also indicating that they do not reflect higher bands.

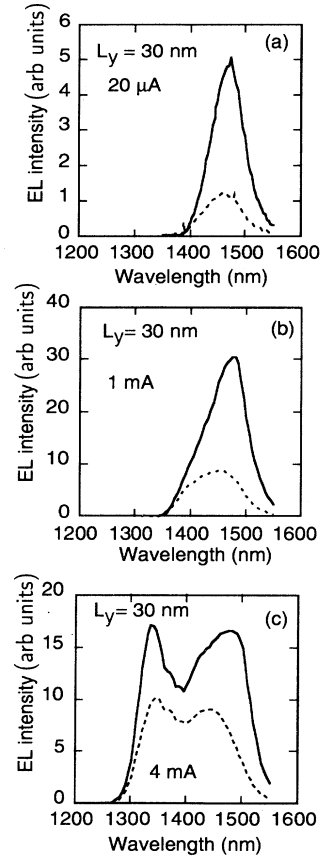


FIG. 18. Injection-current dependence of polarization-resolved EL spectra at 7 K for 30-nm-wide and 15-nm-thick quantum wires: (a) $20 \mu\text{A}$, (b) 1 mA, and (c) 4 mA. Solid and broken lines represent TE and TM polarizations, respectively.

When we regard the EL signal as a transition of the heavy-hole-like band, the observed polarization change seems to be explained as a transition from a two-dimensional to a one-dimensional electronic system. Besides the quantum-confinement effect, the change in the waveguide structures—that is, the change in the volume ratio of the wire region to the InP current-block region—could also affect the polarization of EL through the change of refractive-index modulation. However, if such an effect were dominant, one would expect that the polarization of the QWF's drastically differ from that of the widest wires. (Note that even the 60-nm-wide wires have 90-nm-wide spaces.) The results shown in Fig. 17, however, indicate that such an effect is negligible in our experiment (probably because the volume of the wire region is smaller than that of the waveguide layer). The overall wire-width dependence of the polarization shown in Fig. 17 is therefore intrinsic to the wire structures.

C. Comparison with theory

The polarization of QWW's in contrast to that of QWF's, is well known to be dominated by the valence-band mixing.⁴⁷ Thus mixing has to be adequately taken into account in this study. We calculated the polarization dependence of the optical transition in $\text{In}_{0.53}\text{Ga}_{0.47}\text{As}/\text{InP}$ QWW's incorporating the mixing effect by using the $\mathbf{k}\cdot\mathbf{p}$ method developed in Sec. III. We calculated the momentum matrix element of (110)-oriented $\text{In}_{0.53}\text{Ga}_{0.47}\text{As}/\text{InP}$ QWW's for each polarization. Figure 19 shows the calculated squared-momentum matrix element ($|M|^2$) for the lowest valence band versus the wave vector in the x direction, k_x . In this graph, we assume L_y is 30 nm and L_z is 15 nm.

The curve denoted by calc. 1 in Fig. 17 shows the TM/TE ratio of the squared-momentum matrix element at the zone center. As shown by this curve, the polarization ratio decreases as the wire width decreases. This basically explains the overall tendency seen in the experimental results.

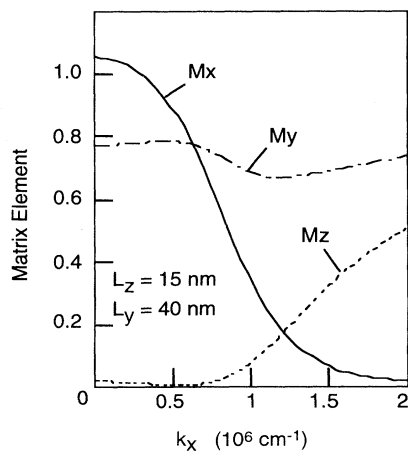


FIG. 19. Calculated wave-vector dependence of the transition matrix elements of 15×40 nm $\text{In}_{0.53}\text{Ga}_{0.47}\text{As}/\text{InP}$ quantum wires for different polarizations.

When L_y is greater, however, a large discrepancy arises. Despite the fact that the theoretical TM/TE ratio is zero for QWF's, the observed TM/TE ratio is 0.166. There are apparently some effects which weaken the anisotropy when L_y is large. We propose two factors to account for this phenomenon. The first is an intrinsic factor that arises from contributions outside the zone center due to finite carrier filling. However, the experimental TM/TE ratio cannot be explained this way even if we consider the region in which $k_x \neq 0$, since the calculated TM/TE does not exhibit strong k_x -dependence at a k_x less than 10^6 cm^{-1} (which corresponds to a 3D carrier concentration of $2-10 \times 10^{18} \text{ cm}^{-3}$). The second is the extrinsic factor of TE and TM signal mixing outside the wires; that is, depolarization during propagation in the waveguide, uncertainty in analyzing the polarization of diverging luminescence from the cleaved facet, or a slight misalignment in the experimental setup. We thus assume a constant extrinsic mixing factor of about 0.14 for all wires, as estimated from the experimental results for QWF's. The calculated data are plotted in Fig. 17, with the extrinsic factor of 0.14 (calc. 2) and with the intrinsic factor from carrier filling up to k_F (Fermi wave vector) of $8 \times 10^5 \text{ cm}^{-1}$ (calc. 3). As seen in this figure, there is a fairly good agreement between calc. 2 and the experimental data. Note that, since we assume a wire-size-independent extrinsic factor, the measured wire-size dependence should result from the quantum confinement. Consequently, the wire-width dependence of the perpendicular-to-plane anisotropy in the EL experiment can be understood as a lateral-confinement-induced polarization change.

D. Anisotropy in surface-emitted PL

We also investigated the in-plane polarization dependence of the surface-emitted PL. Figure 20 shows the dependence of surface-emitted PL intensity on the polar-

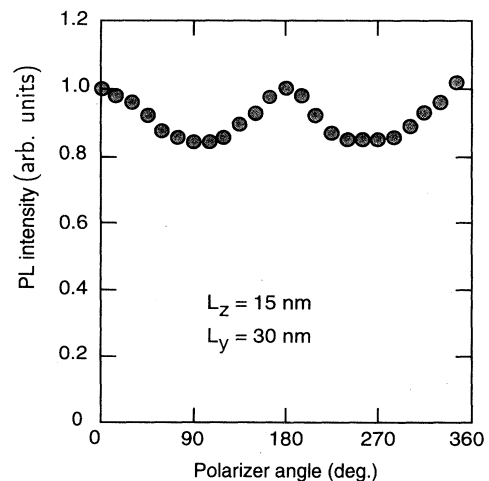


FIG. 20. Polarization dependence of surface-emitted PL signal vs the polarization angle. Zero degrees corresponds to the case where the electric field is parallel to the wire.

izer angle for a 30-nm-wide wire sample. The PL intensity was found to vary sinusoidally with the polarizer angle θ , and to have its largest value when the polarizer was parallel to the wires. The reference QWF's showed no anisotropy in the same configuration.

Figure 21 shows the wire-width dependence of the polarization ratio (P_y/P_x) for surface-emitted PL. Although no anisotropy is observed for the widest wires, PL signals exhibit apparent anisotropy for narrower wires in which the polarization parallel to the wires is strong. The polarization ratio deviates from unity as the wire width decreases to 30 nm. This tendency is consistent with the expected polarization change due to the lateral confinement. However, the results for wires narrower than 25 nm wide cannot be explained simply in terms of the lateral confinement. We will discuss this later in this section.

We compared the above experimental results with the calculations described in Sec. III C 3. The curve denoted calc. 1 in Fig. 21 represents the calculated P_y/P_x . The overall width dependence of the experimental results is similar to the calculated curve down to at least 30 nm. This suggests that the in-plane anisotropy is caused by the lateral confinement in these wire structures. The results of calc. 1 are more polarized than the experimental results for all wire widths. In contrast to the perpendicular-to-plane polarization, the calculated ratio of P_y/P_x exhibits significant k_x dependence even for 1–2-meV carrier filling. Therefore, we have to incorporate a nonzero k_x contribution. The curve denoted calc. 2 represents the calculation with a carrier filling k_F of up to $5.0 \times 10^5 \text{ cm}^{-1}$. Fairly good agreement is obtained between the experimental results and calc. 2 of wires wider than 25 nm. Although we also consider the extrinsic depolarizing factor, it has less of an effect here than in the perpendicular-to-plane case. Calc. 3 represents the

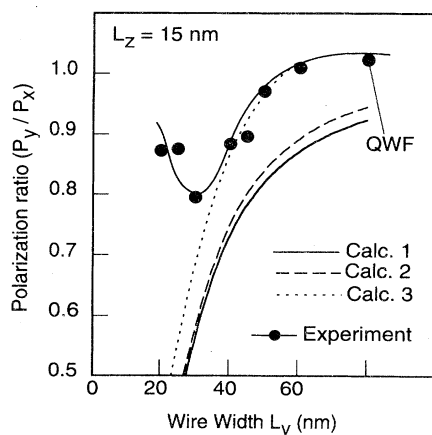


FIG. 21. Wire-width dependence of in-plane polarization ratio in quantum wires. P_y and P_x are luminescence intensities when the electric field is in the y direction (i.e., perpendicular to the wires) and in the x direction (i.e., parallel to the wires), respectively. Curves calculated are also plotted (calcs. 1–3) using three models described in the text. The curve connecting the experimental data is a guide to the eye.

calculation incorporating an extrinsic factor of the same value as in the EL experiment.

This theory does not explain the anomalous phenomenon observed for L_y less than 25 nm. This phenomenon might be explained in terms of wave-function localization in QWW's, as recently discussed.^{48–50} It has been pointed out that wave-function localization, which can be caused by some imperfection (size fluctuation and/or pinning centers at the regrowth interfaces), can weaken the polarization anisotropy in QWW's. Assuming a constant size fluctuation for all wires, we expect that, in narrow wires, when the localization length is comparable to the lateral size, the in-plane anisotropy will be weakened and eventually vanish. Since the polarization property dealt with in this study reflects the heavy-hole-related transitions, holes would be easily localized. Recently, we measured the size fluctuation in QWW's fabricated in the same way,⁵¹ and found that the wire widths are distributed with a standard deviation of 10–20 Å. This is close to the value used in Ref. 49; thus the above explanation is applicable to the QWW's measured here.

A precise calculation of the fluctuation-induced localization would be very complicated since it depends on the detailed characteristics of size fluctuations. We therefore do not proceed with more quantitative studies in this paper. Note, however, that the polarization of edge-emitted signals depends less on the in-line localization than that of surface-emitted ones, because the former is mainly determined by its cross-sectional shape.

VI. SUMMARY

We investigated the optical properties of $\text{In}_{0.53}\text{Ga}_{0.47}\text{As}/\text{InP}$ QWW's while varying the confinement size. The measured wires were fabricated by EB lithography, reverse-mesa wet etching, and metal-organic vapor-phase epitaxy (MOVPE) overgrowth, which is advantageous when varying the lateral size.

We performed PL experiments on these QWW's to analyze the lateral confinement effect. The PL intensity was regained down to a wire width of 35 nm, which is quite different from cases involving dry-etched wires. The wires we fabricated are quite optically active, even at a width of 10 nm. Detailed analysis of the PL results yielded two apparent confirmations of the lateral quantum-confinement effect: one is the PL peak-energy shift with changing wire size down to a 10-nm width, and the other is the appearance of lateral quantized states. The observed PL shift was well explained by energy-level calculations incorporating the excitonic effect. The characteristics of the lateral quantized subbands were also clarified by these calculations.

Magneto-PL measurements in the Faraday configuration were done for the same samples. An intense magnetic field suppressed the blueshift induced by changing the lateral size. In this configuration, magnetic-field-induced confinement is found to compete with the lateral confinement, and so can be used to clarify the origin of the blueshift. The energy-level calculation incorporating the magnetic field well explained the measured results,

confirming that the blueshift is caused by the lateral confinement. In addition, the shoulder structures on the high-energy side of the PL peaks were found to be continuously joined with second Landau subbands as magnetic fields increased, clearly showing that these Landau subbands originated from lateral quantized subbands. We also observed quenching of higher Landau subbands under high-excitation conditions, and this quenching is attributed to an inhibition of the Landau orbit due to the lateral confinement in the wires.

We also investigated the polarization anisotropic property, which is another expected quantum-confinement effect in QWW's. We measured the perpendicular-to-plane anisotropy in edge-emitted EL and the in-plane anisotropy in surface-emitted PL for various lateral wire sizes. Results of both measurements show that polarization properties change according to changes in the cross-sectional shape of the wires. The measured wire-size dependence of the anisotropy was basically explained by

the theoretical calculation. However, a discrepancy was observed for the in-plane anisotropy of very narrow wires, which is thought to be due to the wave function localization.

These confinement-size-dependent optical properties clearly show that a transition from a two-dimensional to a one-dimensional electron-hole system occurs in these QWW's.

ACKNOWLEDGMENTS

We would like to thank M. Naganuma for helping to initiate this work and providing much valuable advice, T. Nishida for developing the nanostructure fabrication process, and T. Mizutani, Y. Imamura, T. Sugeta, and T. Ikegami for giving their encouragement. Part of this work was performed at Grenoble High Magnetic Field Laboratory in France with a great support from M. Potemski.

*Fax: +81 462 40 4305. Electronic address:
notomi@aecl.ntt.jp

¹Y. Arakawa and H. Sakaki, *Appl. Phys. Lett.* **40**, 939 (1982).

²M. Asada, Y. Miyamoto, and Y. Suematsu, *Jpn. J. Appl. Phys. Lett.* **95**, 78 (1985).

³D. Gershoni, H. Temkin, G. J. Dolan, J. Dunsmuir, S. N. G. Chu, and M. B. Panish, *Appl. Phys. Lett.* **53**, 995 (1988).

⁴B. E. Maile, A. Forchel, R. Germann, J. Straka, L. Korte, and C. Thanner, *Appl. Phys. Lett.* **57**, 807 (1990).

⁵J. Y. Marzin, A. Izrael, L. Birotheau, B. Sermage, N. Roy, R. Aoulay, D. Robein, J.-L. Benchimol, L. Henry, V. Thierry-Mieg, F. R. Ladan, and L. Taylor, *Surf. Sci.* **267**, 253 (1992).

⁶H. Asai, S. Yamada, and T. Fukui, *Appl. Phys. Lett.* **51**, 1518 (1987).

⁷S. Tsukamoto, Y. Nagamune, M. Nishioka, and Y. Arakawa, *J. Appl. Phys.* **71**, 533 (1992).

⁸S. A. Chalmers, H. Weman, J. C. Yi, H. Kroemer, J. L. Merz, and N. Dagli, *Appl. Phys. Lett.* **57**, 1751 (1990).

⁹H. Weman, M. S. Miller, C. E. Pryor, Y. J. Li, P. Bergman, P. M. Petroff, and J. L. Merz, *Phys. Rev. B* **48**, 8047 (1993).

¹⁰S. Simhony, E. Kapon, E. Colas, D. M. Hwang, N. G. Stoffel, and P. Worland, *Appl. Phys. Lett.* **59**, 2225 (1991).

¹¹M. Naganuma, M. Notomi, H. Iwamura, M. Okamoto, T. Nishida, and T. Tamamura, *J. Cryst. Growth* **105**, 254 (1990).

¹²M. Notomi, M. Naganuma, T. Nishida, T. Tamamura, S. Nojima, H. Iwamura, and M. Okamoto, *Appl. Phys. Lett.* **58**, 720 (1991).

¹³M. Notomi, M. Okamoto, H. Iwamura, and T. Tamamura, *Appl. Phys. Lett.* **62**, 1094 (1993).

¹⁴M. Notomi, M. Nakao, and T. Tamamura, *Appl. Phys. Lett.* **62**, 2045 (1993).

¹⁵T. P. Smith III, J. A. Brum, J. M. Hong, C. M. Knoedler, H. Arnot, and L. Esaki, *Phys. Rev. Lett.* **61**, 585 (1988).

¹⁶A. S. Plaut, H. Lage, P. Grambow, D. Heitman, K. von Klitzing, and K. Ploog, *Phys. Rev. Lett.* **67**, 1642 (1991).

¹⁷Y. Nagamune, Y. Arakawa, S. Tsukamoto, M. Nishioka, S. Sasaki, and N. Miura, *Phys. Rev. Lett.* **69**, 2963 (1992).

¹⁸H. Weman, E. D. Jones, C. R. McIntyre, M. S. Miller, P. M. Petroff, and J. L. Merz, *Superlatt. Microstruct.* **13**, 5 (1993).

¹⁹I. Suemune, L. A. Coldren, and S. W. Corzine, *Superlatt. Microstruct.* **4**, 19 (1988).

²⁰H. Kanbe, A. Chavez-Pirson, H. Ando, H. Saito, and T. Fukui, *Appl. Phys. Lett.* **58**, 2969 (1991).

²¹J. Hammersberg, H. Weman, M. Notomi, and T. Tamamura, *Superlatt. Microstruct.* **16**, 143 (1994).

²²B. E. Maile, A. Forchel, R. Germann, and D. Grutzumacher, *Appl. Phys. Lett.* **54**, 1552 (1989).

²³A. Forchel, H. Leier, B. E. Maile, and R. Germann, *Festkörperprobleme* **28**, 99 (1988).

²⁴G. Bastard, J. A. Brum, and R. Ferreira, in *Solid State Physics*, edited by H. Ehrenreich and D. Turnbull (Academic, San Diego, 1991), Vol. 44.

²⁵G. A. Baraff and D. Gershoni, *Phys. Rev. B* **43**, 4011 (1991).

²⁶U. Ekenberg, *Phys. Rev. B* **40**, 7714 (1989).

²⁷C. Wetzel, Al. L. Efros, A. Moll, B. K. Meyer, P. Omling, and P. Sobkowicz, *Phys. Rev. B* **45**, 14052 (1992).

²⁸G. Hendorfer, M. Seto, H. Ruckser, W. Jantsch, M. Helm, G. Brunthaler, W. Jost, H. Obloch, K. Köhler, and D. J. As, *Phys. Rev. B* **48**, 2328 (1993).

²⁹Y. Yamauchi, Y. Arakawa, and J. N. Schulman, *Appl. Phys. Lett.* **57**, 1224 (1990).

³⁰R. Chen and K. K. Bajaj, *Phys. Rev. B* **50**, 1949 (1994).

³¹*Semiconductors, Physics of Group IV Elements and III-V Compounds*, edited by O. Madelung, M. Schultz, and H. Weiss, Landolt-Börnstein, New Series, Group III, Vol. 17, Pt. a (Springer-Verlag, Berlin, 1985); *Semiconductors, Intrinsic Properties of Group IV Elements and III-V, II-VI and I-VII Compounds*, edited by O. Madelung, M. Schultz, and H. Weiss, Landolt-Börnstein, New Series, Group III, Vol. 22, Pt. a (Springer-Verlag, Berlin, 1987).

³²T. Yamauchi, T. Takahashi, and Y. Arakawa, *IEEE J. Quan-*

- tum Electron. **QE-27**, 1817 (1991).
- ³³E. O. Kane, *J. Phys. Chem. Solids* **1**, 82 (1956).
- ³⁴S. Nojima, *Phys. Rev. B* **46**, 2302 (1992).
- ³⁵J. W. Brown and H. N. Spector, *Phys. Rev. B* **35**, 3009 (1987).
- ³⁶T. Kodama and Y. Osaka, *Jpn. J. Appl. Phys.* **25**, 1875 (1986).
- ³⁷H. Haug and S. W. Koch, *Quantum Theory of the Optical and Electronic Properties of Semiconductors*, 2nd ed. (World Scientific, Singapore, 1990), Chap. 7.
- ³⁸M. Walther, E. Kapon, D. M. Hwang, E. Colas, and L. Nunes, *Phys. Rev. B* **45**, 6333 (1992).
- ³⁹R. Dingle, W. Wiegmann, and C. H. Henry, *Phys. Rev. Lett.* **33**, 827 (1974).
- ⁴⁰J. Yoshino, H. Sakaki, and T. Hotta, *Surf. Sci.* **142**, 326 (1984).
- ⁴¹L. D. Landau and E. M. Lifshiz, *Quantum Mechanics*, 2nd ed. (Pergamon, Oxford, 1975).
- ⁴²T. Tanaka, Y. Arakawa, and G. Bauer [*Phys. Rev. B* **50**, 7719 (1994)] reported that the calculated 1D magnetoexciton binding energy shows only very slight magnetic-field dependence.
- ⁴³K. F. Berggren, T. J. Thornton, D. J. Newson, and M. Pepper, *Phys. Rev. Lett.* **57**, 1769 (1986).
- ⁴⁴S. Tarucha, H. Okamoto, Y. Iwasa, and N. Miura, *Solid State Commun.* **52**, 815 (1984).
- ⁴⁵M. Sugawara, N. Okazaki, T. Fujii, and S. Yamazaki, *Phys. Rev. B* **48**, 8102 (1993).
- ⁴⁶H. Iwamura, T. Saku, H. Kobayashi, and Y. Horikoshi, *J. Appl. Phys.* **54**, 2692 (1983).
- ⁴⁷P. C. Sercel and K. J. Vahala, *Appl. Phys. Lett.* **57**, 545 (1990).
- ⁴⁸J. Singh, *Appl. Phys. Lett.* **59**, 3142 (1991).
- ⁴⁹T. Tanaka, M. Willatzen, Y. Arakawa, P. Bhattacharya, and J. Singh, *Appl. Phys. Lett.* **62**, 756 (1993).
- ⁵⁰K. Nikolic and A. Mackinnon, *Phys. Rev. B* **47**, 6555 (1993).
- ⁵¹M. Notomi, M. Nakao, and T. Tamamura, *Jpn. J. Appl. Phys.* **32**, 2973 (1993).

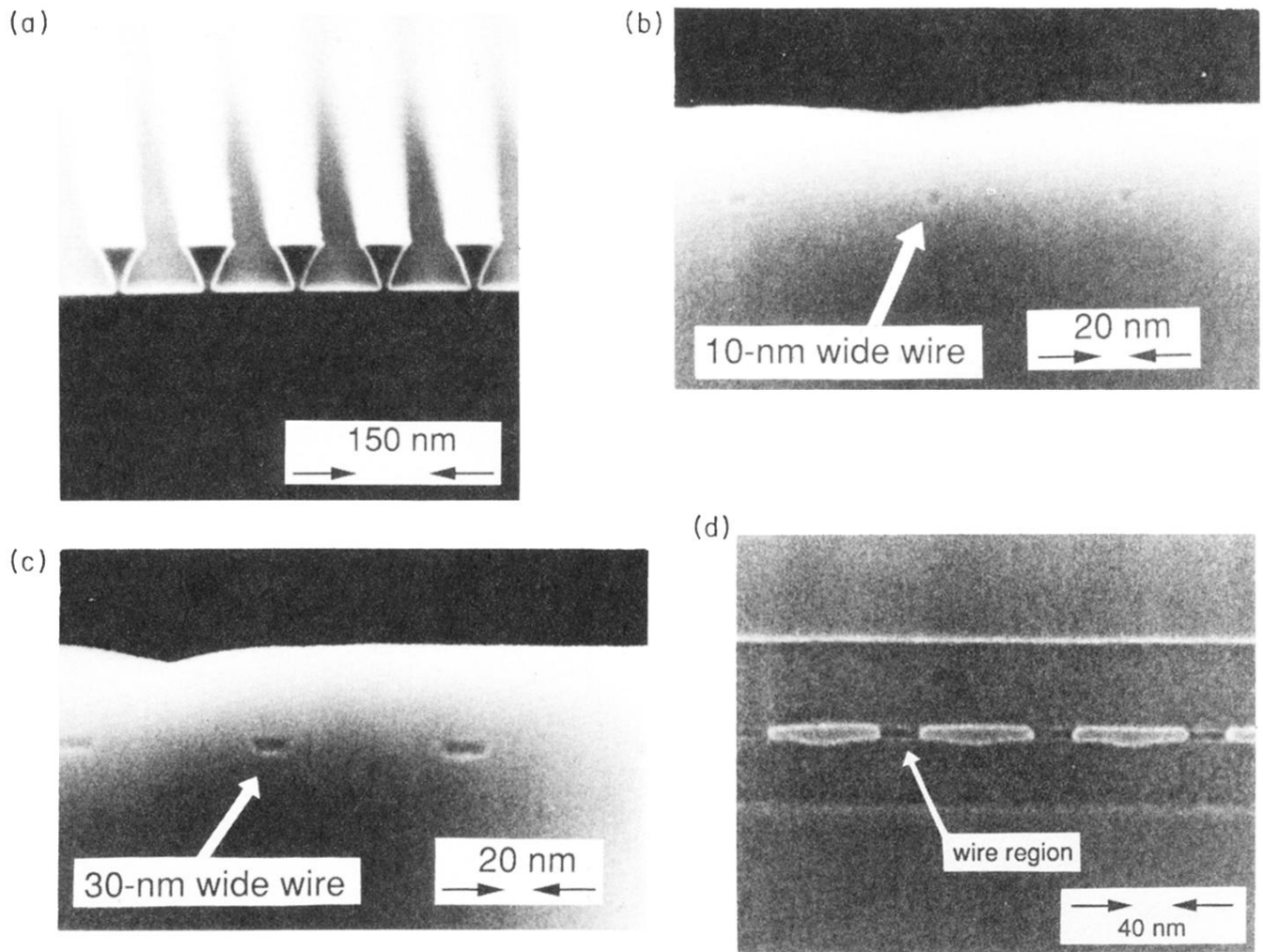


FIG. 2. SEM cross-sectional views of $\text{In}_{0.53}\text{Ga}_{0.47}\text{As}/\text{InP}$ quantum wires. As-etched 10-nm-wide quantum wires (a). Buried 10-nm-wide (b) and 30-nm-wide (c) quantum wires. Quantum wires within the waveguide layer (d).